STRUCTURAL BIOLOGY COMMUNICATIONS

ISSN 2053-230X

The structure of SDS22 provides insights into the mechanism of heterodimer formation with PP1

Meng S. Choy, Nicolas Bolik-Coulon, Tara L. Archuleta, Wolfgang Peti and Rebecca Page*

Chemistry and Biochemistry, University of Arizona, 1041 East Lowell Drive, Biosciences West, Tucson, AZ 85281, USA. *Correspondence e-mail: rebeccapage@email.arizona.edu

Received 11 October 2018
Accepted 19 November 2018

Edited by S. Sheriff, Bristol-Myers Squibb, USA

Keywords: SDS22; protein phosphatase 1; LRR protein; PP1 regulator.

PDB reference: SDS22, 6mky

Supporting information: this article has supporting information at journals.iucr.org/f

Protein phosphatase 1 (PP1) dephosphorylates hundreds of key biological targets by associating with nearly 200 regulatory proteins to form highly specific holoenzymes. The vast majority of regulators are intrinsically disordered proteins (IDPs) and bind PP1 via short linear motifs within their intrinsically disordered regions. One of the most ancient PP1 regulators is SDS22, a protein that is conserved from yeast to mammals. Sequence analysis of SDS22 revealed that it is a leucine-rich repeat (LRR) protein, suggesting that SDS22, unlike nearly every other known PP1 regulator, is not an IDP but instead is fully structured. Here, the 2.9 Å resolution crystal structure of human SDS22 in space group $P2_12_12_1$ is reported. SDS22 adopts an LRR fold with the horseshoe-like curvature typical for this family of proteins. The structure results in surfaces with distinct chemical characteristics that are likely to be critical for PP1 binding.

1. Introduction

Protein phosphatase 1 (PP1), a single-domain protein that is exceptionally well conserved from fungi to humans, is one of the most widely expressed and abundant serine/threonine phosphatases (Brautigan & Shenolikar, 2018). As a consequence, PP1 regulates a diverse set of processes, including carbohydrate metabolism, protein synthesis and cell division, among many others (Cohen, 2002). Although free PP1 has no specificity, in cells PP1 dephosphorylates numerous targets with exquisite specificity. This is achieved via its interaction with ∼200 distinct regulatory proteins, including inhibitory proteins that keep PP1 in an inactive state (such as inhibitor-2) and targeting proteins that form highly specific holoenzymes (such as spinophilin, GADD34, KNL1 and RepoMan) (Peti *et al.*, 2013).

Multiple biochemical and structural studies have revealed that the vast majority of these regulatory proteins bind PP1 via short linear motifs (SLiMs). These SLiMs are between two and eight residues in length, are found within intrinsically disordered regions (IDRs) of the regulators and function to mediate protein–protein interactions. While PP1-specific SLiMs are unstructured in solution, they become ordered when bound to PP1 (Bajaj *et al.*, 2018; Choy *et al.*, 2014, 2015; Ragusa *et al.*, 2010). The first SLiM to be identified in regulators of PP1 was RV*x*F, where *x* represents any amino acid. Subsequent structural studies revealed that this SLiM binds to a deep hydrophobic pocket on PP1 that is ∼20 Å from the catalytic site (Egloff *et al.*, 1997). Since then, additional PP1-specific SLiMs have been identified, including the SILK (Hurley *et al.*, 2007), ΦΦ (O'Connell *et al.*, 2012), Arg (Choy *et al.*, 2014) and KiR (Kumar *et al.*, 2016) SLiMs, which each bind to PP1 at distinct pockets.

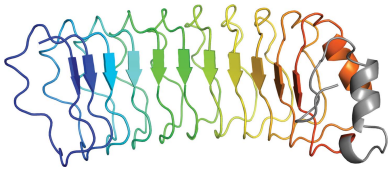

SDS22 is a regulator of PP1 that is conserved from yeast to humans (Fig. 1; Brautigan & Shenolikar, 2018). Upon its discovery nearly 30 years ago, an analysis of the SDS22 sequence revealed that it consists almost entirely of folded leucine-rich repeats (LRRs; Ohkura & Yanagida, 1991). This makes SDS22 unusual among PP1 regulators in that SDS22 is not an intrinsically disordered protein (IDP) but instead is likely to bind PP1 via its folded domain. Consistent with this hypothesis, SDS22 does not contain the RV*x*F SLiM that is present in nearly 85% of all known PP1 regulators. Further, in 2002, yeast two-hybrid studies showed that mutations in the folded domain of SDS22 disrupt PP1 binding (Ceulemans *et al.*, 2002). SDS22 has also been shown to form a trimeric complex with both PP1 and a second PP1 regulator, inhibitor-3 (I-3; Pedelini *et al.*, 2007). More recently, SDS22 has been shown to regulate PP1-mediated dephosphorylation of Aurora B kinase (Eiteneuer *et al.*, 2014) and promote the folding of PP1 into its active conformation upon protein synthesis (Weith

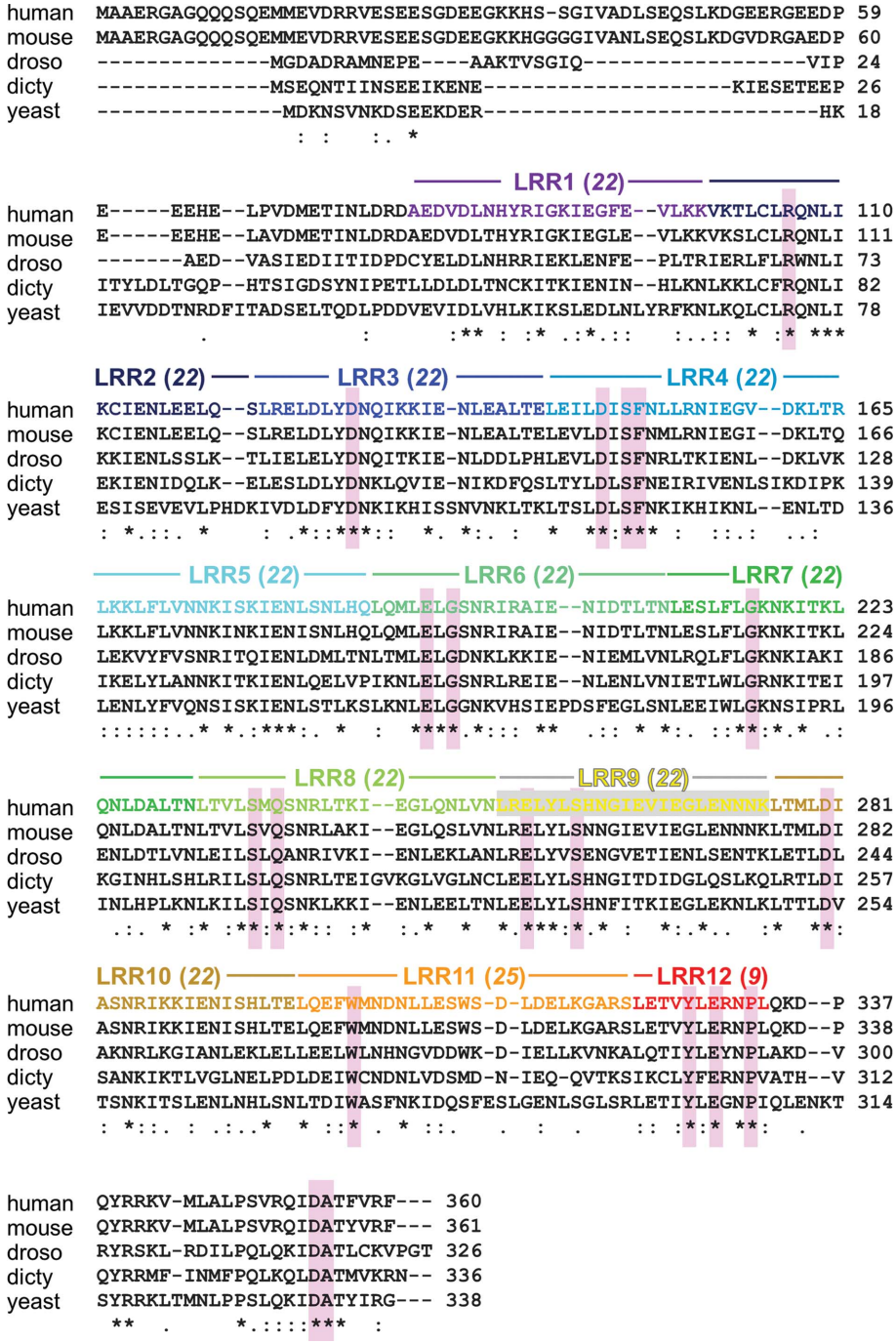

Figure 1
SDS22 sequence alignment. Sequence alignment of SDS22s from various species [human, mouse, *Saccharomyces cerevisiae* (yeast), *Drosophila melanogaster* (droso) and *Dictyostelium discoideum* (dicty)]. The LRRs are indicated using the color code from Fig. 4(*a*). The most highly conserved residues that are not part of the LRR core, as determined from an alignment of SDS22s from 39 distinct species, are shaded in pink.

et al., 2018). Here, we describe the crystal structure of human SDS22 in a $P2_12_12_1$ crystal form and show how the regular LRRs in SDS22 result in biophysically distinct surfaces; these surfaces, coupled with the crystal contacts that SDS22 makes with itself in the asymmetric unit, reveal new insights into the likely mechanism by which SDS22 complexes with PP1.

2. Materials and methods

2.1. Macromolecule production

2.1.1. Plasmid construction. The SDS22 (56–360; UniProt ID Q15435) gene was cloned into a modified pcDNA3.4 vector (pcDNA3.4_K_RP1B). The pcDNA3.4_K_RP1B vector contains a Kozak consensus sequence, an N-terminal 6×His tag, a TEV cleavage site and a multiple cloning site (the latter elements are derived from the *Escherichia coli* RP1B expression vector; Peti & Page, 2007) following the pcDNA3.4 human cytomegalovirus (CMV) promoter. This plasmid was amplified and purified using the PureLink HiPure Plasmid Maxiprep Kit (ThermoFisher).

2.1.2. Protein expression. The recombinant protein was expressed in Expi293F cells (ThermoFisher) at a ratio of 1.0 µg DNA per millilitre of final transfection-culture volume. Transfections were performed using 600 ml in 2 l baffled flasks according to the manufacturer's protocol. The Expi293F cells were cultured in Gibco Expi293 Expression Medium (ThermoFisher) in a humidified incubator at 37°C and 6.5% CO_2 with shaking at 125 rev min^{-1}. On the day of transfection, the Expi293F cell density was between 3 and 5 × 10^6 cells ml^{-1}. Prior to transfection, the Expi293F cells were seeded at 2.9 × 10^6 cells ml^{-1} in 85% of the final transfection volume. SDS22 (56–360) DNA was mixed with Opti-MEM Reduced Serum Medium (ThermoFisher); in a separate tube, Expifectamine reagent (ThermoFisher) was mixed with Opti-MEM medium. These mixtures were incubated separately for 5 min, after which the DNA and Expifectamine mixtures were combined and incubated for an additional 20 min. The final transfection mixture was then added to the cells. Enhancer 1 and Enhancer 2 were added to the cells 18–20 h post-transfection. After an additional 24–28 h, the cells were harvested and the pellet was stored at −80°C.

2.1.3. Protein purification. The cell pellet was resuspended in ice-cold lysis buffer (25 m*M* Tris pH 8.0, 0.5 *M* NaCl, 5 m*M* imidazole, 0.1% Triton X-100) with one cOmplete Mini EDTA-free protease-inhibitor cocktail tablet (Sigma). The resuspended cells were lysed using an Avestin Emulsiflex 3C high-pressure homogenizer at 10.3 MPa. The cell lysate was clarified by centrifugation at 40 000*g* for 45 min and the resulting supernatant was filtered using a 0.22 µm syringe filter (Millipore). The filtered supernatant was then loaded onto a HisTrap FF column (GE Healthcare) pre-equilibrated with buffer *A* (25 m*M* Tris pH 8.0, 500 m*M* NaCl, 5 m*M* imidazole). The column was washed with buffer *A* until the baseline was reached, followed by a wash with 8% buffer *B* (25 m*M* Tris pH 8.0, 500 m*M* NaCl, 250 m*M* imidazole); after this, the protein was eluted using a linear gradient of 8–60% buffer *B*. The fractions containing SDS22 were pooled and the His_6 tag was cleaved using tobacco etch viral protease (overnight incubation at 4°C in SDS22 buffer: 20 m*M* Tris pH 8.0, 500 m*M* NaCl, 0.5 m*M* TCEP, 1 m*M* $MnCl_2$). The cleaved His_6 tag and TEV were removed using a second Ni–NTA column. The SDS22 protein was then combined with PP1α_{7-300} (Choy *et al.*, 2014) at various molar ratios and incubated on ice for 60 min, after which the complex was purified using size-exclusion chromatography (Superdex S75 column equilibrated in SDS22 buffer; Fig. 2). The purity of the complex was quantified using SDS–PAGE. The complex was concentrated to 10 mg ml^{-1} for crystallization trials. Macromolecule-production information is summarized in Table 1.

2.2. Crystallization

Initial crystallization trials were performed using Intelli-Plates 96-3 (Art Robbins) and different commercial sparse-matrix screens (JCSG, BCS Eco, LMB and ProPlex) at room temperature and 4°C. The crystals used for data collection and structure determination were obtained at room temperature in hanging-drop Linbro trays (pH adjusted to 7.8; the conditions are described in Table 2). Crystals typically formed within three days. SDS–PAGE of washed crystals showed that they consisted exclusively of SDS22 (subsequent limited digestion studies of the *in vitro* reconstituted SDS22–PP1 complex showed that complex formation renders PP1 unusually susceptible to proteolysis; why this occurs is under active investigation). The crystals were harvested,

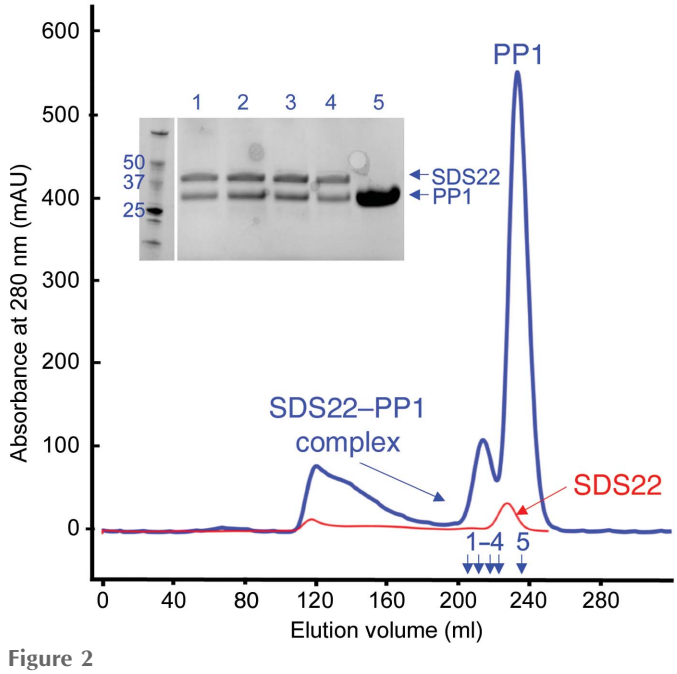

Figure 2
Purification of the SDS22–PP1 complex. Overlay of size-exclusion chromatograms of SDS22 alone (red) and of the SDS22–PP1 complex (blue; 1:5 ratio of SDS22:PP1). The complex elutes before either protein alone (218 ml, complex; 228 ml, SDS22; 235 ml, PP1). Expected molecular masses: SDS22, 36.1 kDa; PP1, 33.9 kDa. An SDS–PAGE of the SDS22–PP1 purification (blue) is shown (samples 1–5 are indicated by arrows).

Table 1
Macromolecule-production information.

Source organism	*Homo sapiens*
Expression vector	pcDNA3.4_K_RP1B
Expression host	HEK293F
UniProt ID	Q15435
Complete amino-acid sequence of the construct produced†	*GHMGSEEDPEEEHELPVDMETINLDRDAED* *VDLNHYRIGKIEGFEVLKK*VKTLCLRQN LIKCIENLEELQSLRELDLYDNQIKKIE NLEALTELEILDISFNLLRNIEGVDKLT RLKKLFLVNNKISKIENLSNLHQLQMLE LGSNRIRAIENIDTLTNLESLFLGKNKI TKLQNLDALTNLTVLSMQSNRLTKIEGL QNLVNLRELYLSHNGIEVIEGLENNNKL TMLDIASNRIKKIENISHLTELQEFWMN DNLLESWSDLDELKGARSLETVYLERNP LQKDPQYRRKVMLALPSVRQIDATFVRF

† Residues not modeled owing to a lack of electron density are shown in italics.

Table 2
Crystallization.

Method	Hanging-drop vapor diffusion
Plate type	24-well Linbro plate
Temperature (K)	298
Protein concentration (mg ml^{-1})	10
Buffer composition of protein solution	20 m*M* Tris pH 8.0, 500 m*M* NaCl, 0.5 m*M* TCEP, 1 m*M* $MnCl_2$
Composition of reservoir solution	0.1 *M* HEPES pH 7.8, 0.2 *M* ammonium sulfate, 0.01 *M* cadmium chloride hemi(pentahydrate), 25%(*v*/*v*) PEG Smear Medium
Volume and ratio of drop	3 µl; 1:2 condition:protein
Volume of reservoir (ml)	0.5

cryoprotected using mother liquor supplemented with 30%(*v*/*v*) glycerol and immediately flash-cooled in liquid nitrogen.

2.3. Data collection and processing

Crystallographic data were collected on beamline 12-2 (wavelength of 0.98 Å) at the Stanford Synchrotron Radiation Lightsource (SSRL) and were processed using *autoXDS* (*XDS*, *AIMLESS* and *TRUNCATE*; Table 3) to a resolution of 2.9 Å (Gonzolez & Tsai, 2010; Kabsch, 2010; Evans & Murshudov, 2013).

2.4. Structure solution and refinement

The structure was determined using molecular replacement (with *Phaser* as implemented in *PHENIX*; Adams *et al.*, 2010; McCoy *et al.*, 2007). PDB entry 4awa (Dall & Brandstetter, 2013) was used as a search model (the N- and C-terminal caps were deleted and the number of central LRRs was extended from eight to 11; 22% identity; selected using *FFAS*; Xu *et al.*, 2014), resulting in a translation *Z*-score of 16.4. *AutoBuild* as implemented in *PHENIX* was used to improve the initial molecular-replacement model. The model was completed using multiple cycles of building and refinement using *Coot* and *phenix.refine*, respectively (Fig. 3). The data and coordinates were deposited in the PDB with PDB entry 6mky. Structure-solution and refinement statistics are given in Table 4.

Table 3
Data collection and processing.

Values in parentheses are for the outer shell.

Diffraction source	Beamline 12-2, SSRL
Wavelength (Å)	0.97946
Temperature (K)	100
Detector	PILATUS 6M, Dectris
Crystal-to-detector distance (mm)	520.5
Rotation range per image (°)	0.15
Total rotation range (°)	200
Exposure time per image (s)	1
Space group	$P2_12_12_1$
a, *b*, *c* (Å)	75.1, 76.5, 128.3
α, β, γ (°)	90, 90, 90
Mosaicity (°)	0.1
Resolution range (Å)	38.27–2.90 (3.08–2.90)
Total No. of reflections	124116 (19788)
No. of unique reflections	16949 (2677)
Completeness (%)	99.6 (99.5)
Multiplicity	7.3 (7.4)
$\langle I/\sigma(I)\rangle$	10.6 (2.2)
R_{meas}	0.215 (2.86)
$CC_{1/2}$	0.965 (0.423)
Overall *B* factor from Wilson plot (Å^2)	72

Table 4
Structure solution and refinement.

Values in parentheses are for the outer shell.

Resolution range (Å)	37.6–2.90 (2.98–2.90)
Completeness (%)	99.2 (96.0)
No. of reflections, working set	16841
No. of reflections, test set	1738
Final R_{cryst}	0.241 (0.317)
Final R_{free}	0.272 (0.368)
No. of non-H atoms	
Protein	4234
Ion (sulfate)	50
Water	17
Total	4301
R.m.s. deviations	
Bonds (Å)	0.002
Angles (°)	0.458
Average *B* factors (Å^2)	
Protein	76
Ion (sulfate)	91
Water	63
Ramachandran plot†	
Most favored (%)	92.4
Allowed (%)	7.6

† Most favored/allowed definitions as determined using *MolProbity* (Williams *et al.*, 2018).

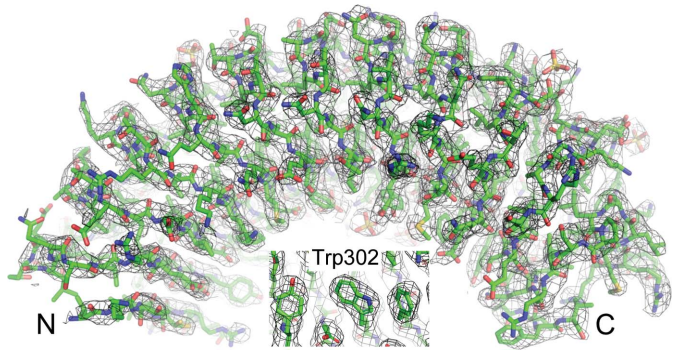

Figure 3
SDS22. $2F_o - F_c$ electron-density map contoured at 1σ (2.9 Å); SDS22 is shown in green. Inset, density for Trp302.

2.5. Sequence alignments

HMMER (Finn *et al.*, 2011) was used to identify and align SDS22 sequences from 39 distinct species. The alignment was then provided to *ConSurf* (Ashkenazy *et al.*, 2016) in order to calculate conservation scores for each amino acid and bin them according to their conservation score. The residues in each bin are given a different color, ranging from dark pink (conserved) to teal (variable), and are plotted as a molecular surface using the SDS22 coordinates in *PyMOL* (Schrödinger; http://www.pymol.org).

3. Results and discussion

We determined the structure of SDS22 residues 100–360, which constitute LRR2–LRR12 and the C-terminal cap [residues 1–88 of SDS22 were previously shown to be dispensable for PP1 binding (Ceulemans *et al.*, 2002), which is consistent with their lack of conservation throughout evolution (Fig. 1)], in space group $P2_12_12_1$. SDS22 adopts the horseshoe fold characteristic of LRR proteins, resulting in both a concave and a convex surface (Fig. 4*a*); the short parallel β-strands in each LRR define the concave surface of

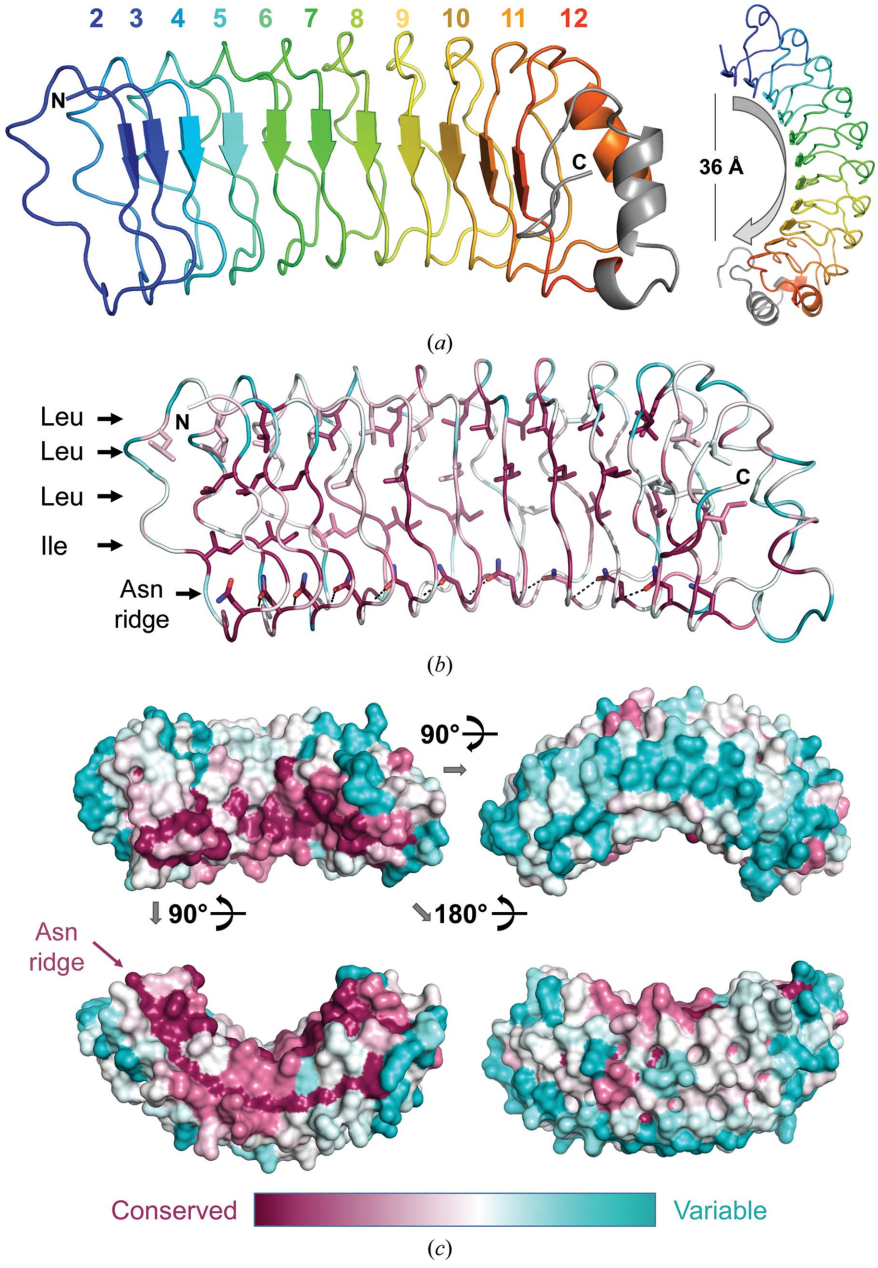

Figure 4
SDS22 structure. (*a*) The structure of SDS22, with the LRRs indicated in distinct colors; the C-terminal cap is in gray. The horseshoe fold characteristic of LRR proteins is evident when viewing the molecule down the LRR β-strands (right). (*b*) An alignment of SDS22 sequences from 39 diverse species was used to identify the residue conservation throughout evolution (most conserved in dark pink to most divergent in teal) and map it onto the SDS22 surface. The majority of the conserved residues define the LRR fold (shown as sticks), including the hydrophobic core (Leu/Ile) and the Asn ridge. (*c*) Sequence conservation mapped onto the SDS22 surface; only the concave surface [upper left; the same orientation as in (*a*) and (*b*)] has highly conserved residues.

SDS22. The overall curvature of SDS22 is about 180° and spans a distance of ∼36 Å. Thirty-nine SDS22 sequences from a diversity of organisms were used to identify the highly conserved versus variable residues in SDS22 sequences (Fig. 4*b*). As expected, the hydrophobic residues that stabilize the LRR fold are conserved, as are the asparagine residues that form the 'Asn ridge' (Fig. 4*c*). These features are key elements of all LRR proteins and function to define the horseshoe-type fold that is characteristic of this family of proteins (for example, the Asn ridge connects neighboring repeats via side chain-to-main chain hydrogen bonds; Rämisch *et al.*, 2014). However, about 20 residues that are not part of

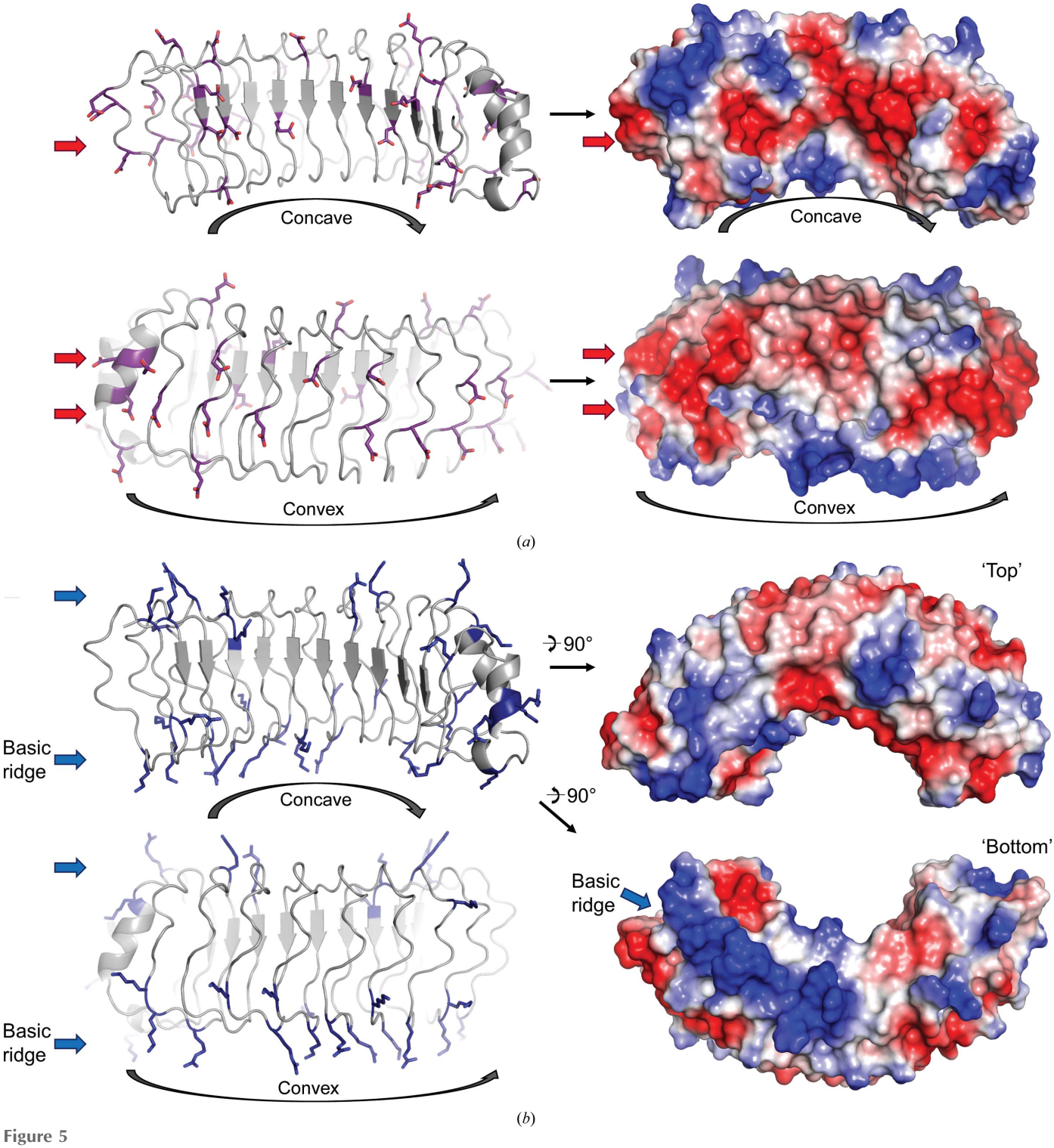

Figure 5
The surface of SDS22 is segregated by charge. (*a*) Acidic residues (Asp and Glu) are shown as sticks (left) and are located primarily on the concave and convex surfaces of SDS22 (right; red, negative; blue, positive). (*b*) Basic residues (Arg and Lys) are shown as sticks (left) and are located on the 'top' and 'bottom' of SDS22 (right). Ten basic residues from LRR2–LRR8 define a particularly distinctive basic patch that we defined as the basic ridge.

the LRR fold are also exceptionally conserved in all 39 sequences. Notably, these are located on the concave surface of SDS22 (Fig. 4*c*, upper left); all other residues are considerably more variable.

Mapping the electrostatic surface onto the surface of SDS22 reveals that the basic arginine/lysine and the acidic aspartic/glutamic acid residues cluster into distinct patches on the surface of SDS22. Both the concave and convex surfaces are characterized by acidic patches (Fig. 5*a*). In contrast, the 'top' and 'bottom' surfaces of SDS22 are characterized by basic patches (Fig. 5*b*). No distinctive hydrophobic patches that may be indicative of a hydrophobic binding pocket are observed.

SDS22 binds PP1 and functions to both promote the folding of PP1 into its active conformation upon protein synthesis (Weith *et al.*, 2018) and regulate the PP1-mediated dephosphorylation of Aurora B kinase (Eiteneuer *et al.*, 2014). An analysis of the asymmetric unit in the $P2_12_12_1$ crystal form provides key additional insights into how SDS22 is likely to associate with PP1. Firstly, as described above, 20 of the most conserved residues in SDS22 are not part of the LRR hydrophobic core. Rather, they are clustered in a single location: the concave surface of SDS22 (Fig. 6*a*). This suggests that they are critical for mediating protein–protein interactions. Because PP1 is also highly conserved throughout evolution, these data suggest that PP1 binds to the concave surface of SDS22. This is consistent with the observation that in most LRR–ligand complexes for which structures have been determined the ligand-binding site is located on the concave surface of the LRR (Bell *et al.*, 2003). Secondly, because two molecules of SDS22 are present in the crystallographic asymmetric unit

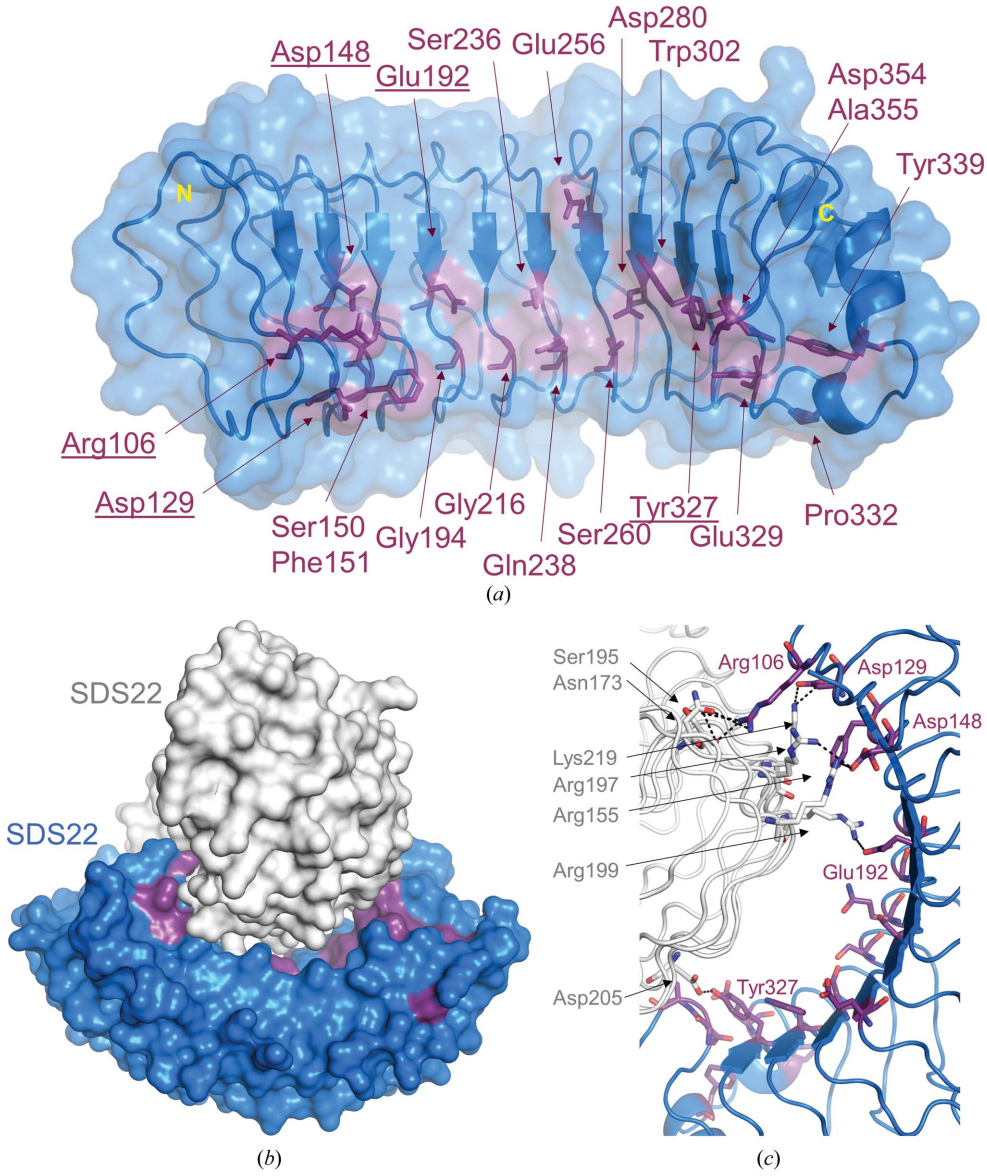

Figure 6
Insights into intermolecular interactions of SDS22. (*a*) The SDS22 residues identified as most conserved that are not part of the LRR hydrophobic core are all located on the concave surface of SDS22 (SDS22, blue surface; the most conserved residues are shown as sticks in dark purple). (*b*) The asymmetric unit of $P2_12_12_1$ SDS22 crystals with SDS22 monomer 1 colored as in (*a*) and monomer 2 in white. (*c*) Close-up of the SDS22 residues that form either salt bridges or hydrogen bonds (black dashed lines).

(Fig. 6*b*), how they interact with one another provides insights into the potential mechanisms used by PP1 to bind SDS22. The two SDS22 molecules in the asymmetric unit are essentially identical, superimposing with a root-mean-square deviation of 0.46 Å. In the crystal, the first molecule of SDS22 binds to the second via its concave surface, burying more than 1800 Å^2 of solvent-accessible surface area (BSA; Tina *et al.*, 2007). Although SDS22 is a monomer in solution, as determined by gel-filtration chromatography, this BSA value is in the range observed for bona fide intermolecular interactions. Because PP1 is globular, with dimensions similar to the concave curvature of SDS22, and because the concave surface is the location of the most highly conserved residues in SDS22, it is most likely that PP1 also binds to the concave surface of SDS22.

The intermolecular interactions between the two SDS22 molecules in the asymmetric unit are exclusively electrostatic/polar. The residues from the concave surface of SDS22 that mediate these interactions are the most highly conserved residues (Fig. 6*c*; Arg106, Asp129, Asp148, Glu192 and Tyr327). They form both salt bridges and hydrogen bonds with residues from the second molecule of SDS22 that include residues from the basic ridge (Arg155, Arg197, Arg199 and Lys219). Because eight of the 20 most highly conserved residues are charged, it is highly likely that charge–charge interactions play a role in PP1 binding, a hypothesis that is consistent with the interface observed between the two molecules of SDS22. Although achieving a full understanding of how SDS22 binds PP1 and how this complex facilitates the interaction of PP1 with other PP1-specific regulators will require additional structural and biophysical characterization, the structure described here represents a key step in achieving this goal.

Acknowledgements

This research used beamline 12.2 at the Stanford Synchrotron Radiation Lightsource. Use of the Stanford Synchrotron Radiation Lightsource, SLAC National Accelerator Laboratory is supported by the US Department of Energy, Office of Science and Office of Basic Energy Sciences under Contract No. DE-AC02-76SF00515. The SSRL Structural Molecular Biology Program is supported by the DOE Office of Biological and Environmental Research and by the National Institutes of Health, National Institute of General Medical Sciences (including P41GM103393).

Funding information

This work was supported by grants from the National Institute of Neurological Disorders and Stroke (R01NS0560128) to WP and from the National Institute of General Medical Sciences (R01GM098482) to RP.

References

Adams, P. D., Afonine, P. V., Bunkóczi, G., Chen, V. B., Davis, I. W., Echols, N., Headd, J. J., Hung, L.-W., Kapral, G. J., Grosse-Kunstleve, R. W., McCoy, A. J., Moriarty, N. W., Oeffner, R., Read, R. J., Richardson, D. C., Richardson, J. S., Terwilliger, T. C. & Zwart, P. H. (2010). *Acta Cryst.* D**66**, 213–221.

Ashkenazy, H., Abadi, S., Martz, E., Chay, O., Mayrose, I., Pupko, T. & Ben-Tal, N. (2016). *Nucleic Acids Res.* **44**, W344–W350.

Bajaj, R., Bollen, M., Peti, W. & Page, R. (2018). *Structure*, **26**, 1327–1336.

Bell, J. K., Mullen, G. E. D., Leifer, C. A., Mazzoni, A., Davies, D. R. & Segal, D. M. (2003). *Trends Immunol.* **24**, 528–533.

Brautigan, D. L. & Shenolikar, S. (2018). *Annu. Rev. Biochem.* **87**, 921–964.

Ceulemans, H., Vulsteke, V., De Maeyer, M., Tatchell, K., Stalmans, W. & Bollen, M. (2002). *J. Biol. Chem.* **277**, 47331–47337.

Choy, M. S., Hieke, M., Kumar, G. S., Lewis, G. R., Gonzalez-DeWhitt, K. R., Kessler, R. P., Stein, B. J., Hessenberger, M., Nairn, A. C., Peti, W. & Page, R. (2014). *Proc. Natl Acad. Sci. USA*, **111**, 4097–4102.

Choy, M. S., Yusoff, P., Lee, I. C., Newton, J. C., Goh, C. W., Page, R., Shenolikar, S. & Peti, W. (2015). *Cell. Rep.* **11**, 1885–1891.

Cohen, P. T. W. (2002). *J. Cell Sci.* **115**, 241–256.

Dall, E. & Brandstetter, H. (2013). *Proc. Natl Acad. Sci. USA*, **110**, 10940–10945.

Egloff, M. P., Johnson, D. F., Moorhead, G., Cohen, P. T., Cohen, P. & Barford, D. (1997). *EMBO J.* **16**, 1876–1887.

Eiteneuer, A., Seiler, J., Weith, M., Beullens, M., Lesage, B., Krenn, V., Musacchio, A., Bollen, M. & Meyer, H. (2014). *EMBO J.* **33**, 2704–2720.

Evans, P. R. & Murshudov, G. N. (2013). *Acta Cryst.* D**69**, 1204–1214.

Finn, R. D., Clements, J. & Eddy, S. R. (2011). *Nucleic Acids Res.* **39**, W29–W37.

Gonzolez, A. & Tsai, Y. (2010). *AUTOXDS*. http://smb.slac.stanford.edu/facilities/software/xds/#autoxds_script.

Hurley, T. D., Yang, J., Zhang, L., Goodwin, K. D., Zou, Q., Cortese, M., Dunker, A. K. & DePaoli-Roach, A. A. (2007). *J. Biol. Chem.* **282**, 28874–28883.

Kabsch, W. (2010). *Acta Cryst.* D**66**, 125–132.

Kumar, G. S., Gokhan, E., De Munter, S., Bollen, M., Vagnarelli, P., Peti, W. & Page, R. (2016). *Elife*, **5**, e16539.

McCoy, A. J., Grosse-Kunstleve, R. W., Adams, P. D., Winn, M. D., Storoni, L. C. & Read, R. J. (2007). *J. Appl. Cryst.* **40**, 658–674.

O'Connell, N., Nichols, S. R., Heroes, E., Beullens, M., Bollen, M., Peti, W. & Page, R. (2012). *Structure*, **20**, 1746–1756.

Ohkura, H. & Yanagida, M. (1991). *Cell*, **64**, 149–157.

Pedelini, L., Marquina, M., Ariño, J., Casamayor, A., Sanz, L., Bollen, M., Sanz, P. & Garcia-Gimeno, M. A. (2007). *J. Biol. Chem.* **282**, 3282–3292.

Peti, W., Nairn, A. C. & Page, R. (2013). *FEBS J.* **280**, 596–611.

Peti, W. & Page, R. (2007). *Protein Expr. Purif.* **51**, 1–10.

Ragusa, M. J., Dancheck, B., Critton, D. A., Nairn, A. C., Page, R. & Peti, W. (2010). *Nature Struct. Mol. Biol.* **17**, 459–464.

Rämisch, S., Weininger, U., Martinsson, J., Akke, M. & André, I. (2014). *Proc. Natl Acad. Sci. USA*, **111**, 17875–17880.

Tina, K. G., Bhadra, R. & Srinivasan, N. (2007). *Nucleic Acids Res.* **35**, W473–W476.

Weith, M., Seiler, J., van den Boom, J., Kracht, M., Hülsmann, J., Primorac, I., Del Pino Garcia, J., Kaschani, F., Kaiser, M., Musacchio, A., Bollen, M. & Meyer, H. (2018). *Mol. Cell*, **72**, 766–777.

Williams, C. J., Headd, J. J., Moriarty, N. W., Prisant, M. G., Videau, L. L., Deis, L. N., Verma, V., Keedy, D. A., Hintze, B. J., Chen, V. B., Jain, S., Lewis, S. M., Arendall, W. B., Snoeyink, J., Adams, P. D., Lovell, S. C., Richardson, J. S. & Richardson, D. C. (2018). *Protein Sci.* **27**, 293–315.

Xu, D., Jaroszewski, L., Li, Z. & Godzik, A. (2014). *Bioinformatics*, **30**, 660–667.